A Novel Intensity Similarity Metric with Soft Spatial Constraint for a Deformable Image Registration Problem in Radiation Therapy

Ali Khamene[1], Darko Zikic[2], Mamadou Diallo[1], Thomas Boettger[3], and Eike Rietzel[4]

[1] Imaging and Visualization Dept., Siemens Corporate Research, Princeton NJ, USA
[2] Computer Aided Medical Procedures (CAMP), TU Munich, Germany
[3] Oncology Care Systems, Siemens Healthcare Sector, Heidelberg, Germany
[4] Particle Therapy, Siemens Healthcare Sector, Erlangen, Germany

Abstract. In this paper we propose a novel similarity metric and a method for deformable registration of two images for a specific clinical application. The basic assumption in almost all deformable registration approaches is that there exist explicit correspondences between pixels across the two images. This principle is used to design image (dis)similarity metrics, such as sum of squared differences (SSD) or mutual information (MI). This assumption is strongly violated, for instance, within specific regions of images from abdominal or pelvic section of a patient taken at two different time points. Nevertheless, in some clinical applications, it is required to compute a smooth deformation field for all the regions within the image including the boundaries of such regions. In this paper, we propose a deformable registration method, which utilizes a priori intensity distributions of the regions delineated on one of the images to devise a new similarity measure that varies across regions of the image to establish a smooth and robust deformation field. We present validation results of the proposed method in mapping bladder, prostate, and rectum contours of computer tomography (CT) volumes of 10 patients taken for prostate cancer radiotherapy treatment planning and verification.

1 Introduction and Background

We address the problem of registering two images and determining the dense deformation field mapping one image to the other. Registration of pairs of medical images (2D or 3D) has been extensively studied (see [9]). In all these approaches, the main assumption is that an image (dis)similarity metric can be established, which can evaluate the quality of a deformation field. Furthermore, the deformation field is required to be continuous, smooth and invertible, so that every pixel in image one (fixed or target) maps to exactly one pixel in image two (moving or template), and vice-versa. The smoothness property can be enforced through regularization of the dense deformation field assuming diffusive [5], elastic [1], viscous fluid [3], or splines [11] properties.

G.-Z. Yang et al. (Eds.): MICCAI 2009, Part I, LNCS 5761, pp. 828–836, 2009.

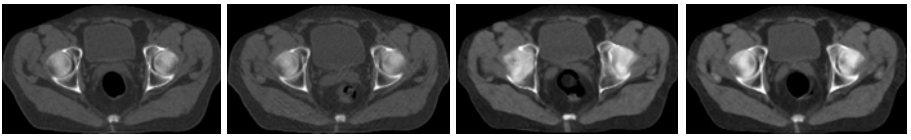

Fig. 1. Figure depicts from left to right, a planning CT slice, a treatment CT slice, the warped version of a treatment CT slice based on a conventional method with SSD as the similarity measure, and the same image done based on the proposed method

A problem arises when, for some parts within the images, no correspondences can be established across the two. This happens quite often while registering medical images. One example is during the registration of CT images from a male pelvis taken for prostate cancer radiotherapy. Rectum and intestine (bowel) content may change drastically from the planning to the treatment sessions. This makes the process of establishing correspondences impossible and more importantly meaningless. There are two problems with the conventional approaches. First is that intensity based similarity metric can not be used for these specific (special) regions within these images. This is mainly due to excessive penalizing effects that they impose on the deformation field within these regions (see Figure 1). If used, this causes erroneous results for the deformation field within these regions. Second, the regularization constraint, and the associated smoothing effect it has, causes the erroneous deformation field to spread to the neighboring areas. The combination intensifies the problem and results an overall unsatisfactory deformation field. This problem is also identified in Foskey et. al. [6], where a two step registration is proposed to deal with the presence of gas in the rectum. We believe that a good approach for solving this problem should be based on a unified variational formulation that can recover the dense deformation field and also deal with these special regions. Joint registration and segmentation approaches have also been proposed, for example in [12] and [4]. However, in [12], the approach only produces deformation fields on the border of the regions (contour in 2D or surface in 3D). In [4] also there is no explicit consideration for the special regions, where no match can exist. We propose a variational registration framework that incorporates statistical intensity constraints on the regions suspected to not have a one-to-one correspondences within the other image. We formulate the problem as a non-linear optimization to solve for the dense deformation, which is based on a combination of a conventional and the region based intensity similarity metric and a classic regularization constraint to enforce smoothness globally on the deformation field.

2 Deformable Registration: Problem Formulation

We consider the problem of deformable registration, where an unknown transformation $\mathcal{T} : \Omega_m \rightarrow \Omega_f$ which maps the intensity images I_m: $\Omega_m \rightarrow \Re$ (i.e., moving) to $I_f : \Omega_f \rightarrow \Re$ (i.e., fixed) defined over the space Ω ($\Omega \in \Re^k$ for $k = 2$ or 3). We assume to have outlines of special regions specified on the fixed image.

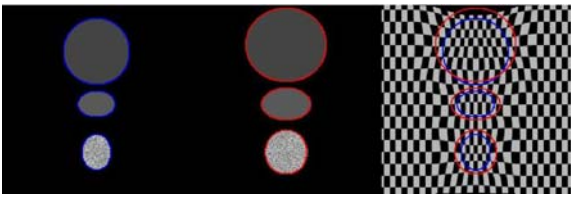

Fig. 2. Figure shows two images (from left) with three deformable objects and their corresponding contours. The lower object in both images contains random distribution of intensities inside, where the pixel-to-pixel correspondences does not exist across the two. Third image (right) shows the desired deformation, which maps the region boundaries and provides a smooth deformation within and on the boundaries of the lower object.

We compartmentalize Ω_f to a set of non-overlapping regions Φ_f^i for $i \in [0, n-1]$, where Φ_f^0 denotes the region, where matching pairs can be found (i.e., majority of image pixels) and Φ_f^i for $i \neq 0$, where matching pairs can not be established. We assume the contours enclosing regions Φ_f^i for $i \neq 0$ are known for I_f and denoted by $C_i^f \in \Omega_f$. We are looking for the transformation $\mathcal{T}$ with the following properties (see Figure 2):

- For any point in the fixed image with in the region Φ_f^0, there should be a corresponding point in the moving image (i.e., $\mathbf{x}_f = \mathcal{T}(\mathbf{x}_m)$ for $\mathbf{x}_f \in \Phi_f^0$).
- A point on the contour of C_i^f for $i \neq 0$ should map to a point on a closed contour denoted as C_i^m for $i \neq 0$ (i.e., $C_i^f = \mathcal{T}(C_i^m)$ for $i \neq 0$). It is important to emphasize that this is only a boundary constraint and does not enforce having correspondences within these regions.
- The transformation $\mathcal{T}$ should be smooth.

3 Proposed Solution

We use the classic two term energy functional for solving this problem. We reformulate the transformation $\mathcal{T}$ as $\mathcal{T}(\mathbf{x}) = \mathbf{x} + \mathbf{u}(\mathbf{x})$, where $\mathbf{u}$ is the displacement (deformation) field. We use various image (dis)similarity terms (i.e., $\mathcal{M}_{\Phi_i}$) depending on the region and one overall deformation smoothness constraint (i.e., $\mathcal{R}$), as follows:

$$\hat{\mathbf{u}} = \arg\min_{\mathbf{u}} \sum_i \beta_i \mathcal{M}_{\Phi_i}(I^f, I^m) + \alpha \int_\Omega \mathcal{R}(\mathbf{u}(\mathbf{x}))d\mathbf{x}, \tag{1}$$

where β_i for $i \in [0, n-1]$ needs to be specified empirically. Furthermore, α signifies the level of smoothness in the deformation field. For region Φ_0, where the correspondences can be found, we could use conventional similarity metrics such as MI [9] or SSD as follows:

$$\mathcal{M}_{\Phi_0}(I^f, I^m) = \int_{\Phi_0} |I^f(\mathbf{x}) - I^m(\mathbf{x} + \mathbf{u}(\mathbf{x}))|^2 d\mathbf{x}. \tag{2}$$

For other regions, we propose to use region based similarity metric with no specific spatial information. We assume that the a priori intensity distributions for these regions are known. This information for example can be established based on outlining various regions within several training data sets. Let us assume that the a priori intensity distribution of the region Φ_i for $i \in [1, n-1]$ is denoted by p_i, we can then define a log likelihood based regional energy constraint as follows:

$$\mathcal{M}_{\Phi_i}(I^f, I^m) = -\sum_i \int_{\Phi_i} log(p_i(I^m(\mathbf{x} + \mathbf{u}(\mathbf{x}))) d\mathbf{x}. \tag{3}$$

It is noteworthy to mention that there is no notion of correspondences present in this equation. The regional energy is minimized for the deformation field, which maps the certain area within the moving image into the region with a known intensity distribution. For example, in a special case, where p_i is a Gaussian distribution, the equation 3 is favoring deformation fields that cause the intensity mean of the mapped region be close to the mean of the a priori distribution. The intensity distribution could either be estimated based on the I_f alone, or it could be estimated using the same image regions from a number patients' scans. The latter is a more reliable option, however can only be used for quantitative imaging modalities such as CT. Finally, as the global deformation regularization, we simply use the diffusion criterion $\mathcal{R}(\mathbf{u}) = trace(\nabla \mathbf{u}^\top \nabla \mathbf{u})$ where $\top$ denotes the transpose operation. Any other regularizer, such as linear-elastic or curvature [10], could be used as well.

3.1 Numerical Treatment

The optimal deformation field minimizing the energy functional (1) is the solution of the Euler-Lagrange equation of $\alpha \Delta \mathbf{u}(\mathbf{x}) = \mathbf{f}(\mathbf{x})$, with certain boundary conditions [10]. In the proposed case, the right hand side in this equation or the image force is modified according to the regions of the fixed image as follows:

$$\begin{aligned} \mathbf{f}(\mathbf{x}) = \Big(& \beta_0 \mathcal{X}_{\phi_0}(\mathbf{x})(I^f(\mathbf{x}) - I^m(\mathbf{x} + \mathbf{u}(\mathbf{x}))) + \\ & \textstyle\sum_i \beta_i \mathcal{X}_{\phi_i}(\mathbf{x}) \frac{\partial p_i(I^m(\mathbf{x}+\mathbf{u}(\mathbf{x})))}{p_i(I^m(\mathbf{x}+\mathbf{u}(\mathbf{x})))} \Big) \nabla I^m(\mathbf{x} + \mathbf{u}(\mathbf{x})), \end{aligned} \tag{4}$$

where $\mathcal{X}_{\phi_i}(\mathbf{x}) = 1$ for all $\mathbf{x} \in \phi_i$ otherwise $\mathcal{X}_{\phi_i}(\mathbf{x}) = 0$. We require a priori distribution to be differentiable and strictly positive. Furthermore, coefficients β_i should be chosen to decrease the discrepancy in the magnitude of the computed force across the regions specially along the borders. We choose to solve the resultant nonlinear parabolic partial differential equation (PDE) using a semi-backward (implicit) Euler update formula as follows:

$$\mathbf{u}_d^{t+1} = (\mathbf{Id} + \alpha \delta t \mathbf{R})^{-1}(\mathbf{u}_d^t + \delta t \mathbf{f}_d(\mathbf{u}^t)), \tag{5}$$

where square matrix $\mathbf{R}$, with each dimension size equal to the total number of pixels in the image, represents the Laplacian operator Δ and $\mathbf{Id}$ is identity matrix

with the same size as **R**. Furthermore, d denotes the dimension (e.g., 1, 2, or 3), the superscript t is iteration step or time, and δt is the time marching coefficient [10]. The update equation 5 provides a greater stability and faster convergence compared to a simpler forward update formulation [7]. The downside is that it involves inverting a large matrix. To accelerate the inversion, we use a multi-grid method similar to the one outlined in [8].

4 Experimental Results

In this section, we explain the specific clinical application for the proposed method in details. Furthermore, we provide a detailed explanation regarding the input data and the desired output for this specific use case. Furthermore, we explain some implementation details and provide the validation results.

4.1 Adaptive Radiotherapy

During the planning phase in radiation oncology, tumors and the organs at risk are delineated and the dose distribution is planned using these contours. The patient undergoes a fractionated treatment process, where the incremental amount of dose is applied over several days. The original planned dose based on the planning CT is usually not valid throughout the whole treatment process, specifically for deformable targets such as prostate and organs at risk such as bladder and rectum with filling variations [6]. One solution is to acquire CT images prior to treatment in order to better capture the recent state of the anatomy. Two options are then available; first is to change the plan according to the recent state of anatomy, and second is keep the original plan but recompute the accumulated dose based on the current state of anatomy and to re-plan only if the accumulated dose deviates too much compared to the planned dose. Both of these options have pros and cons, however, both require an enabling technology that is to robustly find the corresponding structures (and voxels) between the planning and treatment scans. The main registration challenge here, as explained in the introduction section, is that *there are regions within these two images, where explicit correspondences cannot be established.*

4.2 Validation Results

We have acquired 20 pairs of CT data sets from 10 different patients undergone prostate radiotherapy. The first CT in each pair is the planning CT, where the contours of main three organs (prostate, bladder, and rectum) are available. The second CT in each pair is the treatment CT taken during one treatment session using a Siemens CTVision (Siemens Oncology Care Systems, Concord, CA, USA) within the treatment room. The three mentioned structures are then delineated in all the second CT data sets by expert dosimetrists. The regions of the images, which demonstrate significant intensity and shape variability without correspondence are considered to be the rectum, which is posterior to the

Table 1. Quantitative validation of the warped prostate, bladder, rectum contours as the results of the proposed method

Patient	Prostate			Bladder	Rectum
	ρ_d	ρ_{fd}	s_d (mm)	s_d (mm)	s_d (mm)
1	0.94	0.10	2.5	2.9	3.9
2	0.81	0.22	2.8	3.2	5.3
3	0.89	0.16	2.2	3.0	4.6
4	0.91	0.11	2.0	3.1	4.0
5	0.85	0.20	2.5	3.0	4.8
6	0.84	0.22	2.3	2.5	4.7
7	0.88	0.20	2.4	2.6	4.2
8	0.85	0.28	2.1	2.1	4.0
9	0.81	0.25	2.9	3.3	5.2
10	0.88	0.27	2.0	4.1	4.7
Average	0.87	0.20	2.4	3.0	4.1

Table 2. Quantitative validation of the warped prostate, bladder, rectum contours as the results of the conventional deformable registration algorithm with (a) SSD and (b) MI as (dis)similarity metrics

Patient	Prostate			Bladder	Rectum
	ρ_d	ρ_{fd}	s_d (mm)	s_d (mm)	s_d (mm)
1	0.66(a)/0.70(b)	0.28/0.15	3.9/4.0	5.1/5.2	6.4/5.9
2	0.71/0.54	0.38/0.34	4.0/4.0	4.9/5.2	5.9/6.1
3	0.62/0.75	0.40/0.21	4.0/3.7	4.9/5.1	7.5/8.2
4	0.73/0.69	0.39/0.46	4.1/4.1	4.9/4.8	6.7/7.1
5	0.66/0.52	0.41/0.23	3.8/4.0	5.3/5.0	7.2/5.9
6	0.69/0.53	0.38/0.37	3.7/4.0	5.0/5.0	7.0/6.9
7	0.59/0.61	0.43/0.34	4.3/4.2	5.1/4.7	7.6/6.9
8	0.68/0.62	0.19/0.22	4.5/4.1	5.2/4.8	8.0/7.8
9	0.68/0.59	0.31/0.29	4.9/3.8	4.7/5.2	6.8/6.1
10	0.67/0.71	0.20/0.31	4.3/4.2	4.6/4.9	7.1/6.8
Average	0.66/0.62	0.33/0.29	4.1/4.0	4.9/5.0	7.2/6.8

prostate and large intestine (bowel) that is superior to the bladder (see Figure 3). We used contours of the rectum in planning CT of first 10 pairs to estimate the intensity distribution of the rectum (shown in the Figure 4). We also used rough delineations of the large intestine region superior to the bladder of the first 10 pairs to estimate an intestine intensity distribution. We chose a rather large Parzen window of 35 on the Hounsfield scale to make sure the *pdf* is non-zero and smooth (differentiable) within the entire intensity range. We used the second 10 pairs of data as test data. We performed three sets of experiments. In the experiment set (a), we used the region based similarity metric, where the SSD is used for "regular" regions and the proposed similarity metric is used for the "special" regions delineated as the part of the planning process, in set (b), we used SSD as the intensity distance metric for the entire image, and finally

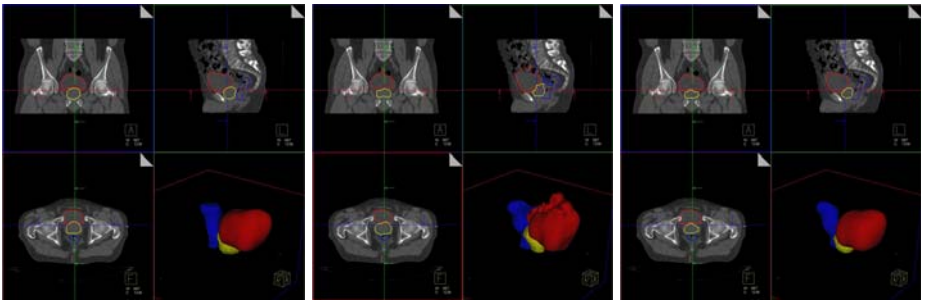

Fig. 3. The figures from left to right are, the treatment CT with ground truth contours of bladder, prostate and rectum, the treatment CT with warped version of the planning contours using a conventional method, and the treatment CT with warped version of the planning contours based on the proposed method

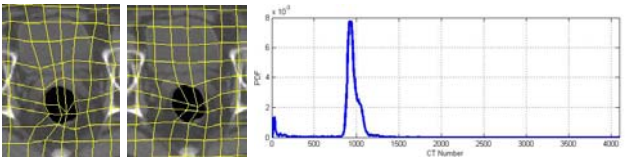

Fig. 4. Two figures on the left show the deformation grid overlaid on the planning data for *left* conventional method, and *right* proposed method. Right figure depicts the *pdf* of the rectum intensity (Hounsfield scale + 1024) based on 10 patient data.

in the set (c), we used MI. We always assume that planning CT is the fixed (reference) and the treatment CT is the moving (template) and we always first rigidly aligned the two images.

The images are all downsampled to $256 \times 256 \times \mathrm{N}$, where N is a number between 96 and 130. In order to cope with large displacements, equation 5 is solved in a scale-space setting. We solved the equations over three levels of resolutions starting with zero displacements as the initial value at the lowest resolution. For the three dimensional images of the mentioned size range, the overall time for registration process in average was less than 30 seconds. For these experiments, we empirically found appropriate values for α, β_0, and β_i once and kept them fixed for the entire test. Within the algorithm, the (dis)similarity metric force is always normalized by the initial (dis)similarity prior to the registration. This relieves us from adjusting the value of the α for various (dis)similarity metrics.

We used the inverse of the computed deformation field computed using the method described in [2] to generate the contours on the treatment data sets. For quantitative evaluation, we used several measures to compare the warped contours based on the registration process with the ground truth delineated by the expert clinician. The quantitative measures where; 1) ρ_d is the probability of detection, calculated as the fraction of the ground truth volume that overlaps with the estimated organ volume, 2)ρ_{fd} is the probability of false detection,

calculated as the fraction of the estimated organ that lies outside the ground truth organ, and 3) s_d is the surface distance, calculated as the average distance between the surfaces of the ground truth and estimated organs. We computed all measures for prostate but only s_d for bladder and rectum. In Tables 1 and 2, we show the measures computed for all three sets of experiments on the patient data. The proposed method always outperformed the conventional approaches, specially by higher margin for the cases where rectum shape changes were significant. Un-smooth deformation fields, which are typical results of the conventional method were problematic for the inverse deformation computation scheme. The examples of a specific patient data set is also brought in Figure 3.

5 Summary and Conclusion

In this paper, we presented a method for deformable registration of images, in a scenario, where there exist areas within the images without explicit correspondences. We take advantage of the assumption that although the pixel-to-pixel correspondence can-not be established, the intensity statistics within these areas remain consistent from image to image. Therefore, we proposed to use a softer region specific intensity matching or similarity constraint on these areas. This problem is clinically prevalent while processing various abdominal and pelvic scans of same patient at different time points. We outlined a detailed scheme for implementing the proposed method and focused on the problem of tumor and organ at risk variability in prostate radiotherapy and demonstrated the performance of the proposed solution.

References

1. Bajscy, R., Lieberson, R., Reivich, M.: A computerized system for the elastic matching of deformed radiographic images to idealized atlas images. J. Comput. Assis. Tomogr. 7, 618–625 (1983)
2. Chen, M., Lu, W., Chen, Q., Ruchala, K.J., Olivera, G.H.: A simple fixed-point approach to invert a deformation field. Med. Phys. 35(1), 81–88 (2008)
3. Christensen, G.E., Joshi, S.C., Miller, M.: volumetric transformation of brain anatomy. IEEE Trans. Medical Image 16, 864–877 (1997)
4. Ehrhardt, J., Schmidt-Richberg, A., Handels, H.: A Variational Approach for Combined Segmentation and Estimation of Respiratory Motion in Temporal Image Sequences. In: Proceedings of ICCV 2007, pp. 14–21 (2007)
5. Fischer, B., Modersitzki, J.: Fast diffusion registration. In: AMS Contemporary Math, Inverse Problems, Image Analysis, and Medical Imaging, vol. 313, pp. 117–129 (2002)
6. Foskey, M., Davis, B., Goyal, L., Chang, S., Chaney, E., Strehl, N., Tomei, S., Rosenman, J., Joshi, S.: Large deformation three-dimensional image registration in image-guided radiation therapy. Phys. Med. Biol. 50, 5869–5892 (2005)
7. Gonzales, C., et al.: Backward Euler Discretization of Fully Nonlinear Parabolic Problems. Mathematics of Computation 71(237), 125–145 (2001)

8. Henn, S., Witsch, K.: Iterative multigrid regularization techniques for image matching. SIAM J. Sci. Comput. 23(4), 1077–1093 (2001)
9. Maintz, J.B.A., Veirgerver, A.: A survey of medical image registration. Medical Image Analysis 2(1), 1–36 (1998)
10. Modersitzki, J.: Numerical Methods for Image Registration. Oxford University Press, New York (2004)
11. Rueckert, D., Frangi, A.F., Schnabel, J.A.: Automatic construction of 3D statistical deformation models using non-rigid registration. In: Niessen, W.J., Viergever, M.A. (eds.) MICCAI 2001. LNCS, vol. 2208, pp. 77–84. Springer, Heidelberg (2001)
12. Unal, G., Slabaugh, G.: Coupled PDEs for non-rigid registration and segmentation. In: Computer Vision and Pattern Recognition - CVPR 2005, vol. 1, pp. 168–175 (2005)